# ECE 796:

# Models of the Neuron

Slides for Lecture #2

Friday, January 19, 2007

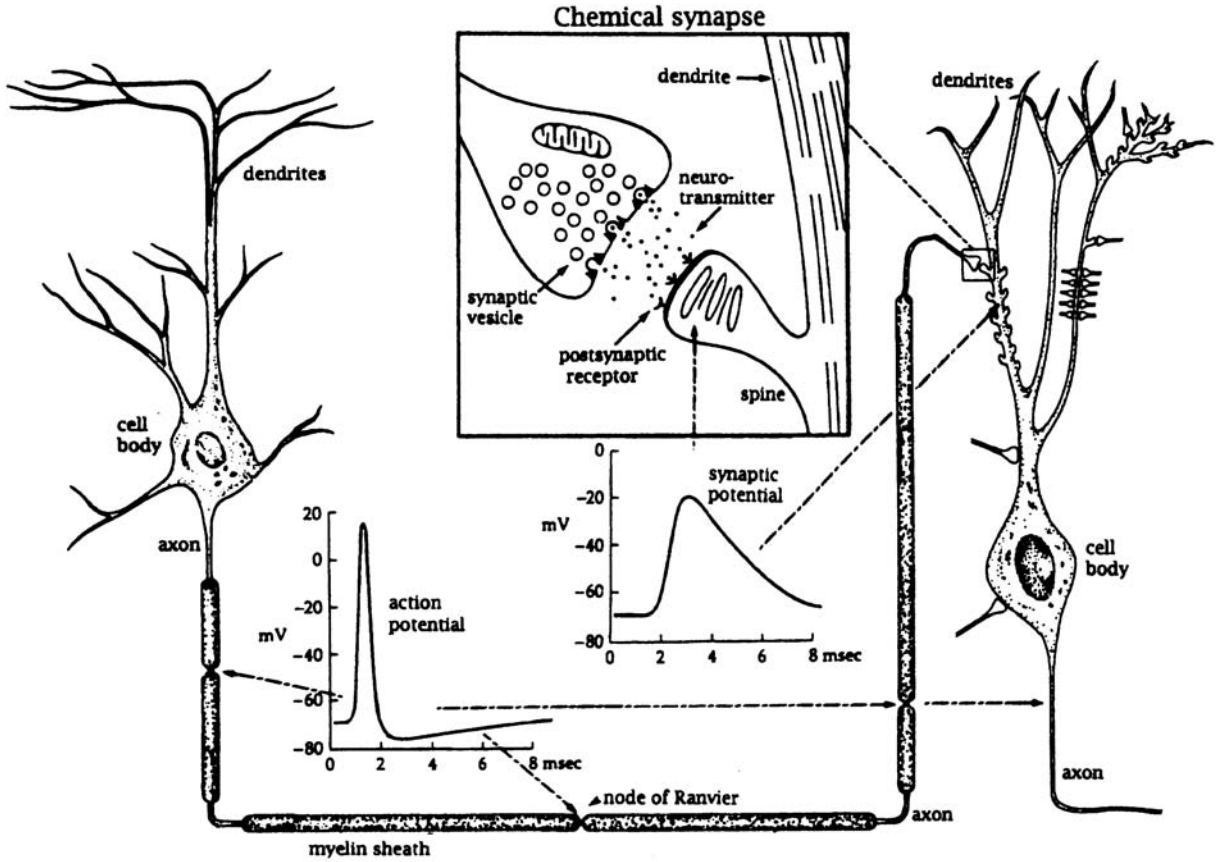


**Figure 1.2** Neurons convey information by electrical and chemical signals. Electrical signals travel from the cell body of a neuron (left) to its axon terminal in the form of action potentials. Action potentials trigger the secretion of neurotransmitters from synaptic terminals (upper insert). Neurotransmitters bind to postsynaptic receptors and cause electric signals (synaptic potential) in the postsynaptic neuron (right). Synaptic potentials trigger action potentials, which propagate to the axon terminal and trigger secretion of neurotransmitters to the next neuron. (Adapted from Kandel et al. 1991 and from L.L. Iversen, copyright © 1979 by Scientific American, Inc. All rights reserved.)

(from Johnston and Wu)

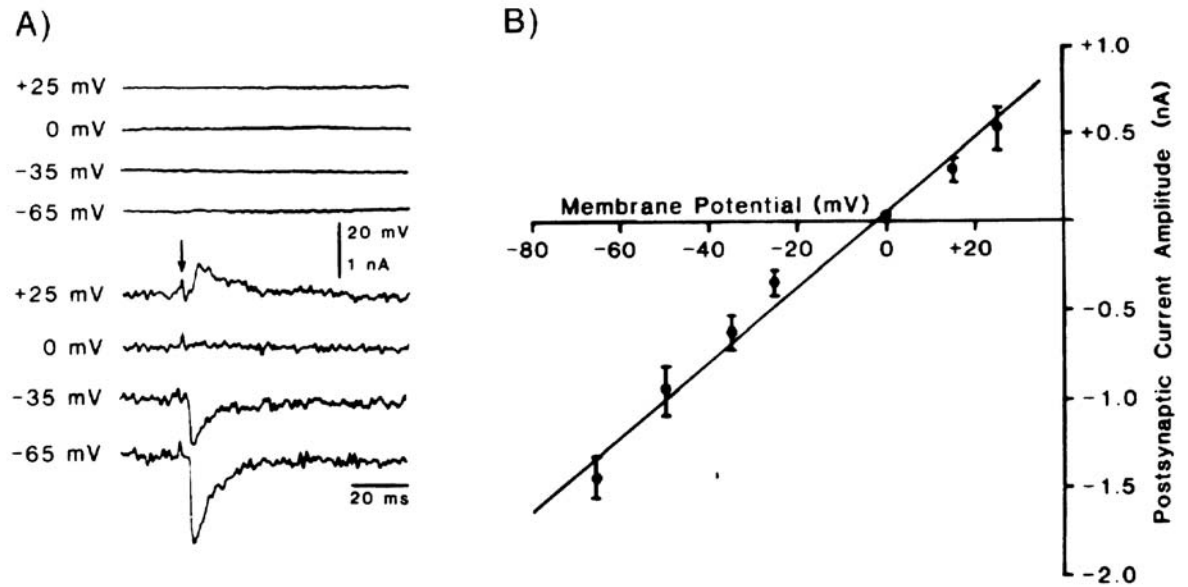


**Fig. 1.6 A Fast Excitatory Synaptic Input** Excitatory postsynaptic current (EPSC) caused by the simultaneous activation of synapses (arrow) made by the mossy fibers onto CA3 pyramidal cells in the rodent hippocampus (Brown and Johnston, 1983). This classical experiment showed how a central synapse can be successfully voltage clamped. **(A)** The voltage-clamp setup stabilizes—via electronic feedback control—the membrane potential at a fixed value. Here four experiments are shown, carried out at the holding potentials indicated at the left. The current that is drawn to keep the membrane potential constant, termed the clamp current, corresponds to the negative EPSC. It is maximal at negative potentials and reverses sign around zero. The synaptic current rises within 1 msec to its peak value, decaying to baseline over 20–30 msec. The experiments were carried out in the presence of pharmacological agents that blocked synaptic inhibition. **(B)** When the peak EPSC is plotted against the holding potential, an approximately linear relationship emerges; the regression line yields an $x$-axis intercept of $-1.9$ mV and a slope of 20.6 nS. Thus, once the synaptic reversal potential is accounted for, Ohm's law appears to be reasonably well obeyed. We conclude that synaptic input is caused by a transient increase in the conductance of the membrane to certain ions. Reprinted by permission from Brown and Johnston (1983).

(from Koch)

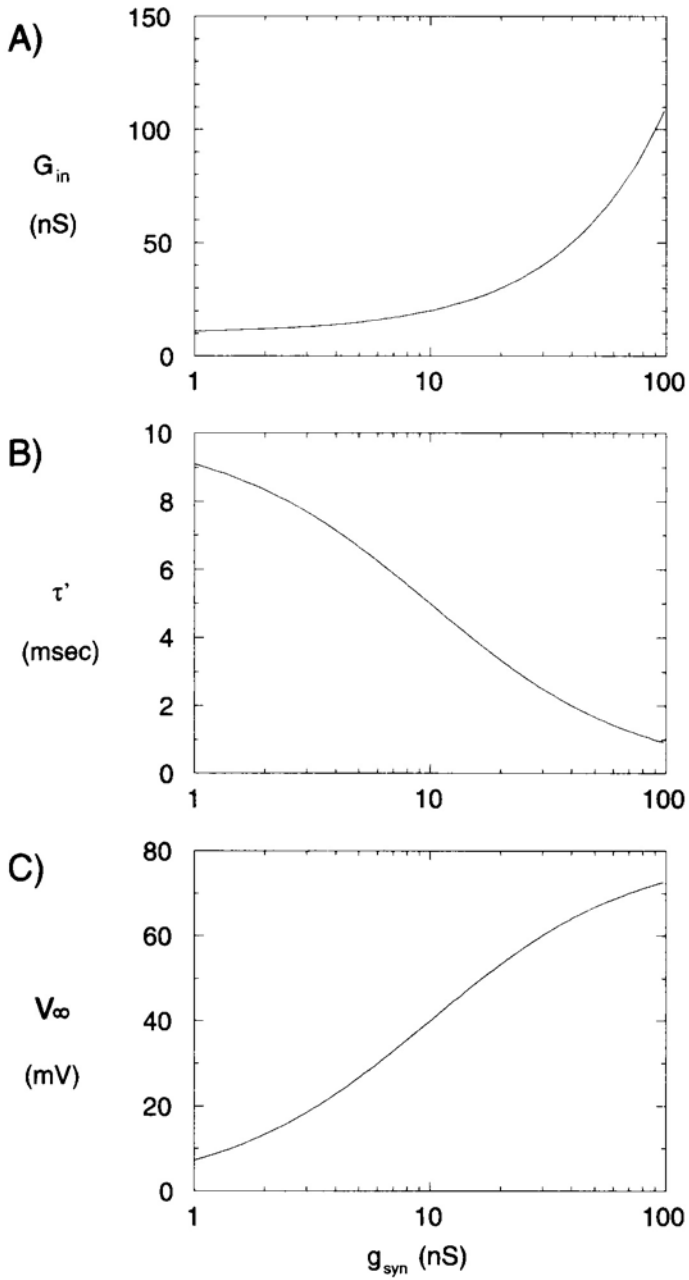


**Fig. 1.9 SYNAPTIC INPUT, SATURATION, AND THE TIME CONSTANT** The effect of varying the synaptic input conductance on **(A)** the input conductance $G_{in}$ (Eq. 1.24), **(B)** the membrane time constant $\tau'$ (Eq. 1.25), and **(C)** the steady-state change in membrane potential $V_\infty$ (Eq. 1.26) in a single-compartment model (Fig. 1.7A) as a function of $g_{syn}$. Conceptually, if we assume an excitatory synapse (with $E_{syn} = 80$ mV) and a fixed peak amplitude of $g_e = 1$ nS, the $x$ axis is logarithmic in the number of synapses involved in the overall synaptic event. Note that $\tau'$ as well as $G_{in}$ will increase irrespective of whether the synapses are depolarizing, shunting, or hyperpolarizing. The fact that the input to neurons comes in the form of a change in the membrane conductance implies that the very structure of the neuronal hardware changes with the input, since the dynamics of the cell speeds up in the presence of strong synaptic input.

(from Koch)

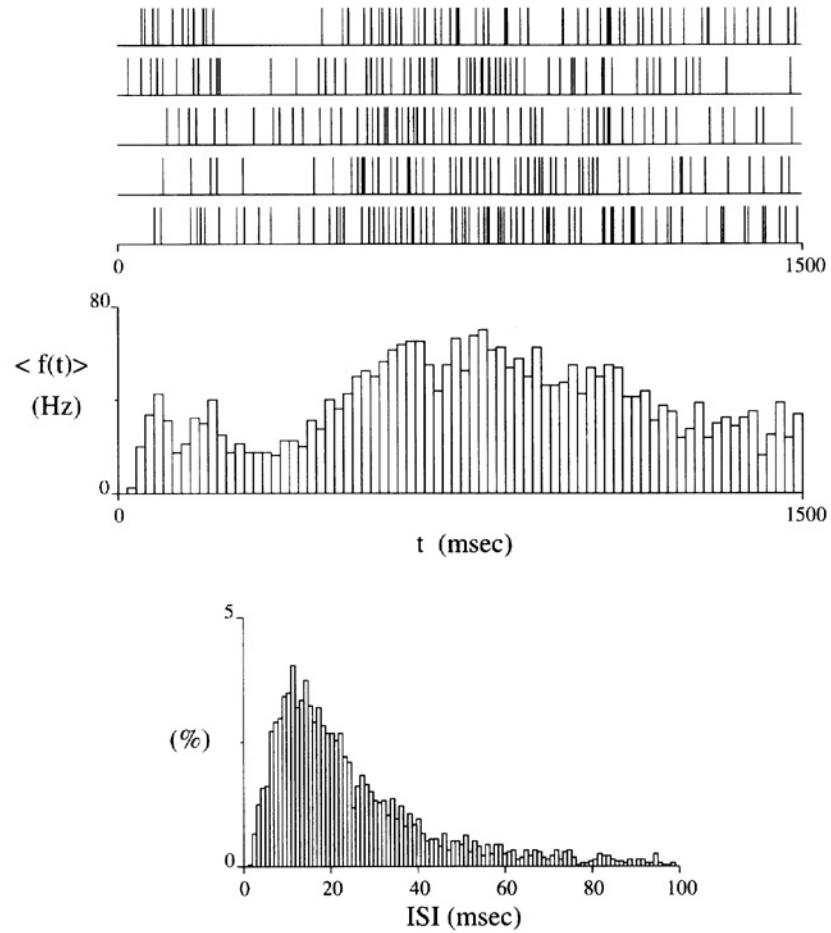


**Fig. 15.1 VARIABILITY OF NEURONAL SPIKING** A high-contrast bar is swept repeatedly over the receptive field of a cortical cell in the awake macaque monkey. Much variability in the microstructure of spiking is evident from trial to trial. The poststimulus time histogram in the middle corresponds to the averaged firing rate $\langle f(t) \rangle$ (using 20 msec bins) taken over 40 trials. The lower plot illustrates the associated interspike interval (ISI) histogram. It shows a lack of very short intervals, indicative of a refractory period, and an exponentially decreasing likelihood of finding very large gaps between spikes. The lack of reproducibility of the detailed spike pattern is the primary reason arguing for the idea of a mean rate code (Eq. 14.1). Yet neurons deep within the cortex can faithfully reproduce the microstructure of spiking over several hours (Fig. 15.11). From W. Newsome, K. Britten, personal communication.

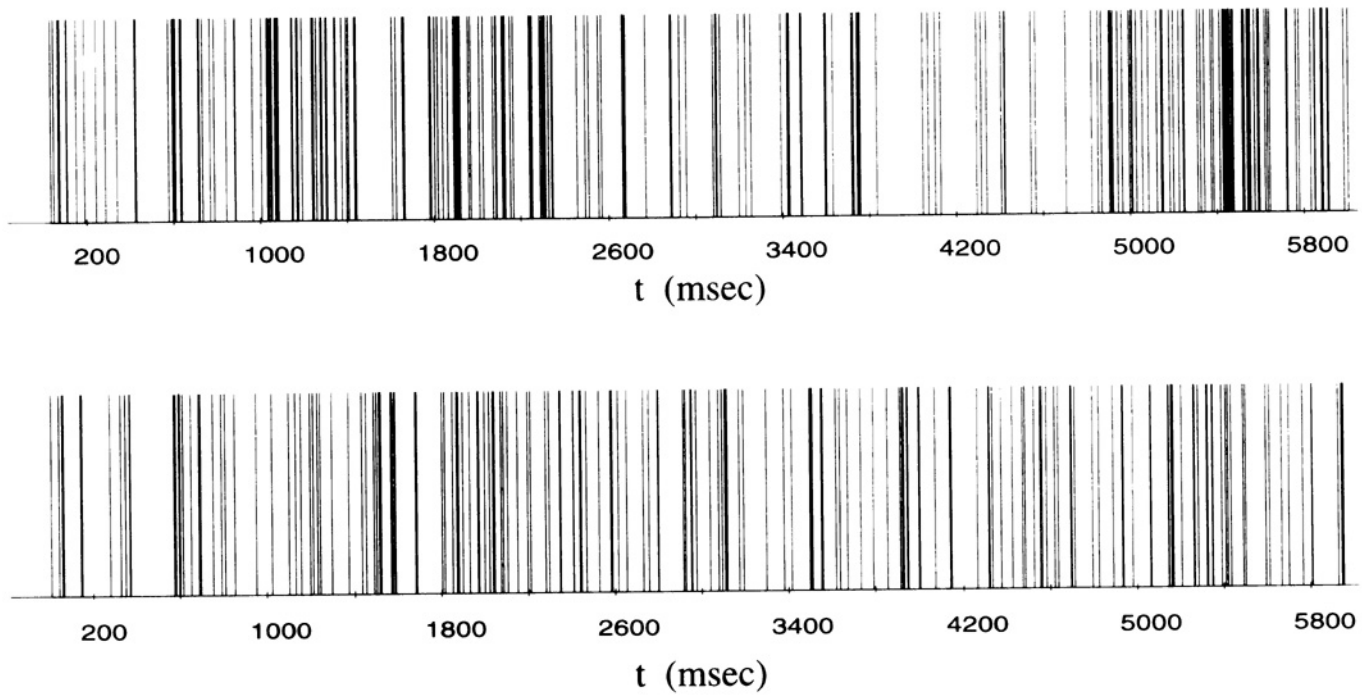


**Fig. 15.2 SPIKE TRAINS AND THE RANDOM POISSON PROCESS** Spike train from an extracellularly recorded cell in the parietal cortex of a behaving monkey (upper trace; data kindly provided by J. Fuster) and from a synthetic Poisson process with a refractory period of 1 msec (lower trace). The mean firing rate of both processes is 30 Hz. Notice the relatively rare occurrences of large gaps between spikes. In a Poisson process, the probability of occurrence of gaps of duration $T$ decreases as $e^{-T\mu}$.

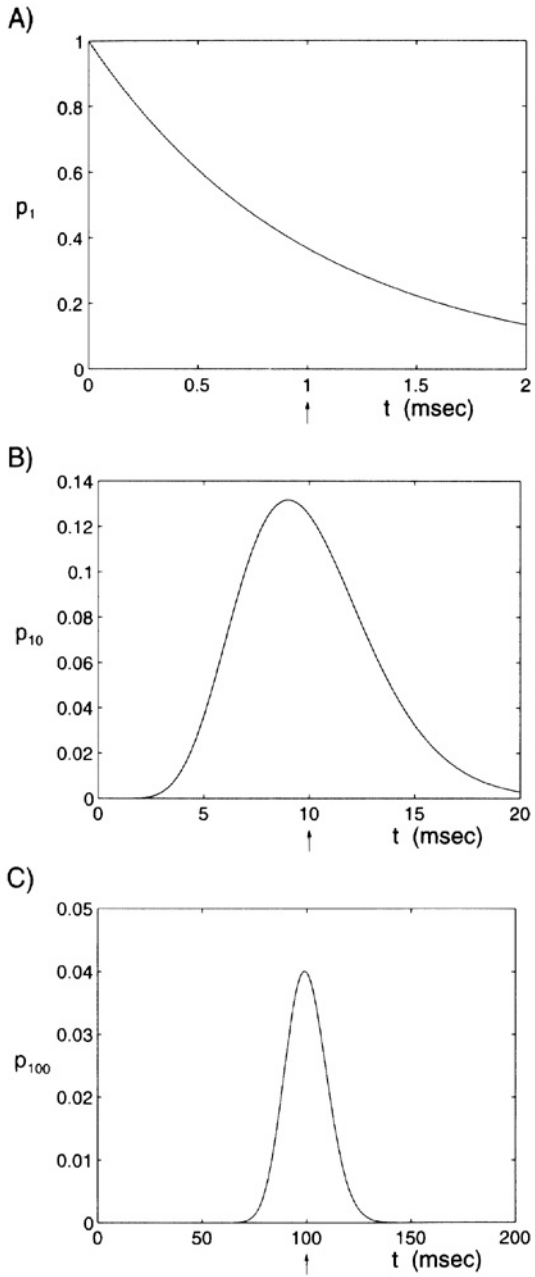


**Fig. 15.4 Interspike Interval Distribution** In the interspike interval distribution the occurrences of the intervals between adjacent spikes is histogrammed. This is done here analytically for pulses generated by a perfect integrate-and-fire unit that receives Poisson distributed input with a constant rate of $\mu = 1000$ (per second). The threshold of the unit varies, with **(A)** $n_{\text{th}} = 1$ (each input generates an output pulse), **(B)** $n_{\text{th}} = 10$, and **(C)** $n_{\text{th}} = 100$. The ISIs are gamma distributed (Eq. 15.12). As expected, the mean output rate decreases as the number of synaptic inputs needed to reach threshold $n_{\text{th}}$ increases (the mean interspike interval is at 1, 10, and 100 msec for the three panels; see arrows). The normalized standard deviation, called the *coefficient of variation* $C_V$ (Eq. 15.15) scales as $1/\sqrt{n_{\text{th}}}$. In other words, the relative jitter in the timing of output pulses becomes smaller as $n_{\text{th}}$ becomes larger. If the cell is integrating over a significant number of small inputs, the ISI distribution approaches the normal distribution (as in **C**).

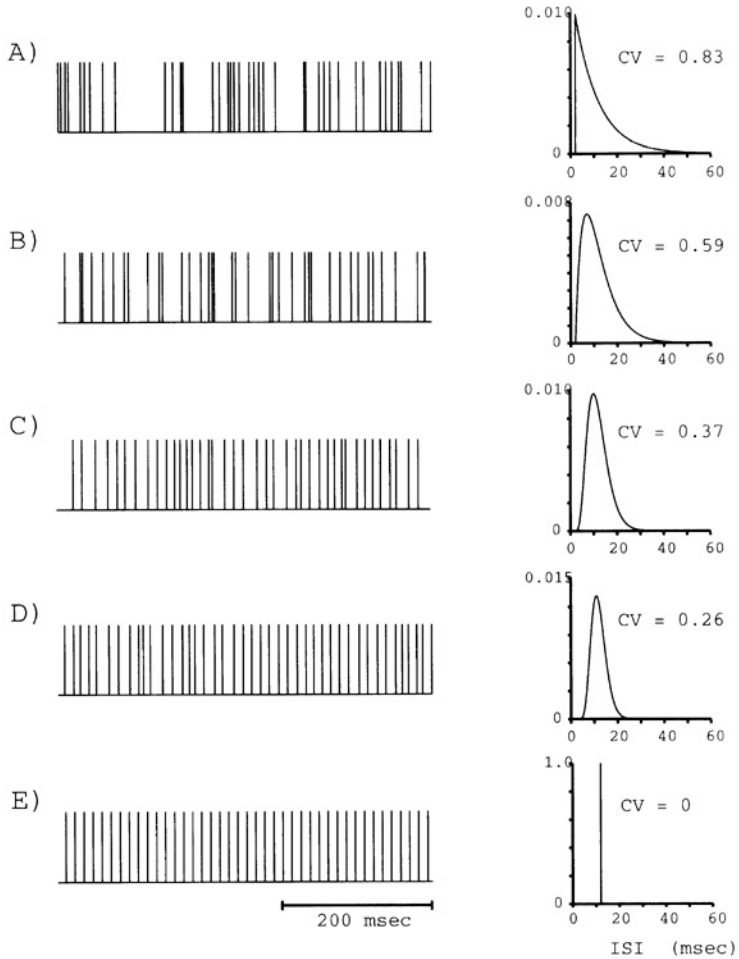


**Fig. 15.5 SPIKE TRAIN INTERSPIKE VARIABILITY** Sample spike trains and interspike interval histograms for a perfect integrator model with an absolute refractory period $t_{\text{ref}}$ of 2 msec for Poisson distributed synaptic input. The mean interspike interval is in all cases identical to 12 msec. **(A)** Each synaptic input gives rise to a spike. The ISI is a shifted exponential; the deviation of the associated $C_V$ from unity reflects the regularizing effect of the refractory period. **(B)–(D)** $n_{\text{th}}$ is increased to 2, 5, and 10, respectively. To retain the same average firing frequency, the input firing frequency was also increased by the same amount. The ISI can be described by a gamma density (Eq. 15.12). **(E)** Response to a sustained current injection.

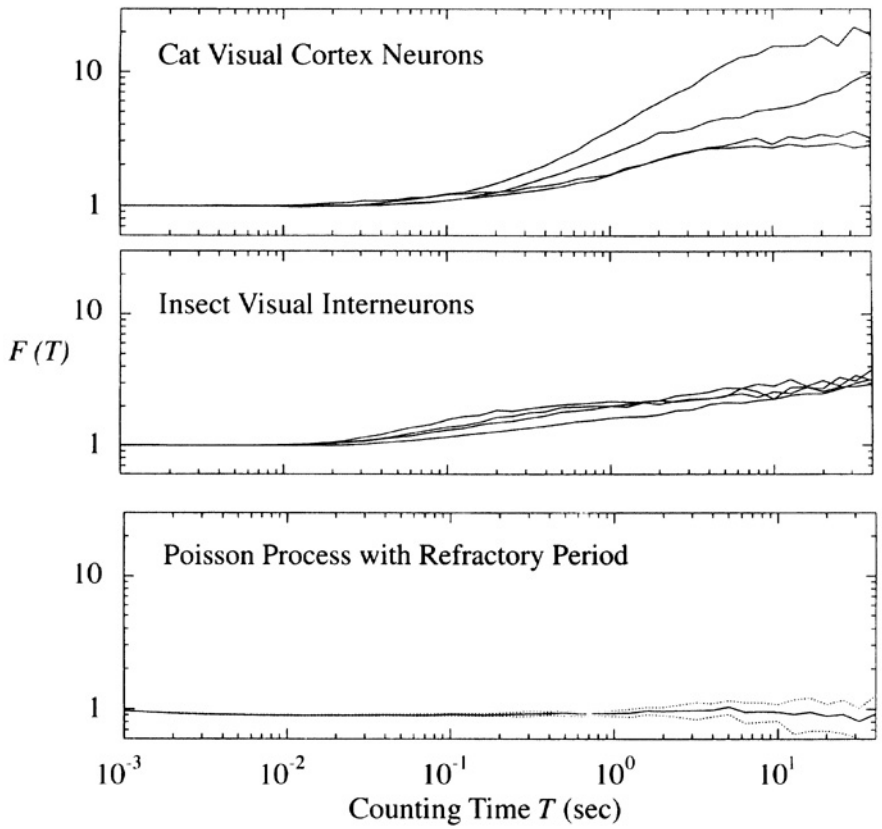


**Fig. 15.6 VARIABILITY IN SPIKE COUNT** Fano Factor (Eq. 15.18), that is, the variance of the number of spikes normalized by their mean, within an observational counting window of duration $T$ in different spiking systems. The top panel shows $F(T)$ for the spontaneous activity of four cells taken from the visual cortex of the anesthetized cat (Teich et al., 1997). For $T < 0.1$ sec, the variability is close to unity, as expected from a Poisson process. However, for larger observational windows, $F(T)$ strongly increases, indicative of long-term correlations in the firing behavior, possibly due to slow state changes in the cat. The qualitatively same behavior for spontaneous activity can be observed in the middle panel, plotting $F(T)$ for four visual interneurons in the cricket (Turcott, Barker, and Teich, 1995), although $F(T)$ is not as large as in the cortex. The lower plot illustrates $F(T)$ (along with its standard deviation) associated with 10 simulated runs of a Poisson process with a refractory period. Since a refractory period imposes some degree of order, $F(T)$ is less than that of a pure Poisson process but still close to unity. Reprinted by permission from Teich, Turcott, and Siegel (1996).

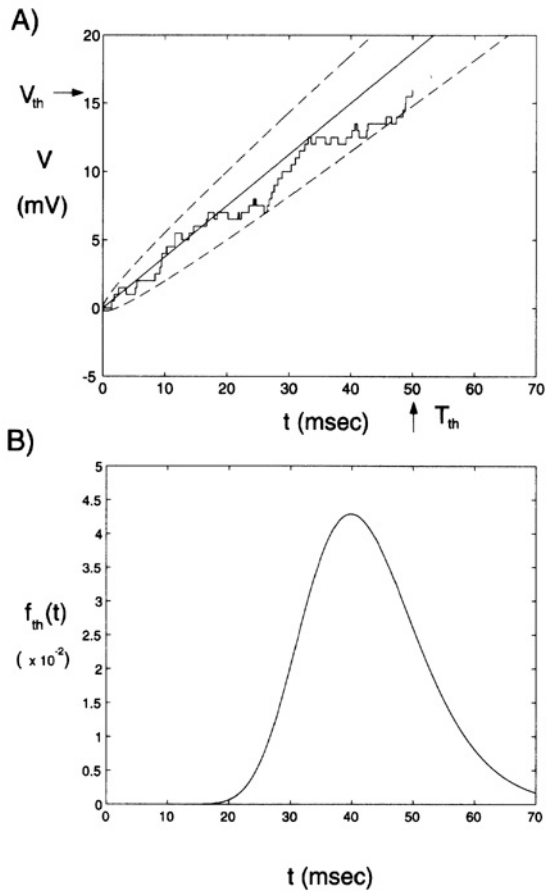


**Fig. 15.7 RANDOM WALK OF THE MEMBRANE POTENTIAL** Illustration of the random walk model of excitatory and inhibitory synaptic input into a nonleaky integrate-and-fire unit as pioneered in this form by Stein (1965). The cell receives Poisson distributed excitatory input (with rate $\mu_e = 1000$ Hz), each increasing the voltage by 0.5 mV, and Poisson distributed inhibitory input (at a rate of 250 Hz), each input decreasing the potential by 0.5 mV. Threshold is reached at 16 mV. **(A)** One instantiation of such a random walk, together with the expected mean potential and its standard deviation. The unit generates a spike at around $T_{\text{th}} = 50$ msec. **(B)** Probability density $f_{\text{th}}(t)$ for the first passage to threshold, that is, for the time it takes before the voltage threshold is reached for the first time.

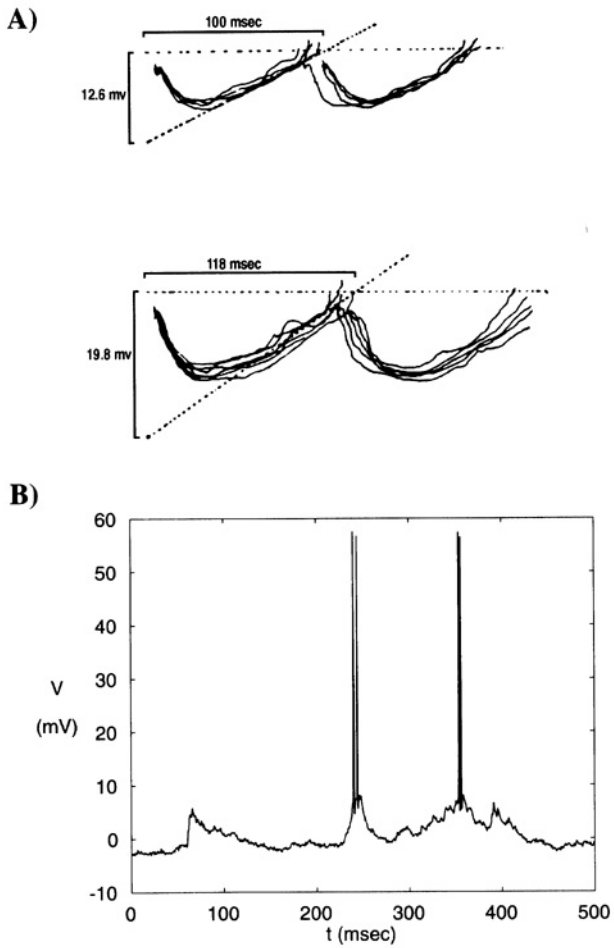


**Fig. 15.8 Does the Membrane Potential Drift up to $V_{th}$?** Intracellular membrane potential in two different cell types. **(A)** Somatic potential in a motoneuron in the spinal cord of an anesthetized cat in response to a constant intracellular current injection (Calvin and Stevens, 1968). Portions of the membrane potential between adjacent spikes are superimposed, matched against a theoretical model in which the depolarization to threshold is expected to be linear in time (Eq. 15.22) and evaluated against a fixed $V_{th}$ (dotted horizontal line). This model explains the jitter in spike timing in two out of five motoneurons investigated entirely on the basis of synaptic input noise. Reprinted in modified form by permission from Calvin and Stevens (1968). **(B)** Intracellular recording from a complex cell in cat visual cortex (Ahmed et al., 1993), responding to a bar moving in the preferred direction. The depolarizing event around 80 msec was not quite sufficient to generate a spike. This cell does appear to integrate over many tens of milliseconds, as witnessed by the slow rise and fall of the membrane potential. It remains a matter of intense debate whether spiking in cortical cells can be explained by treating the cell as integrating over a large number of small excitatory and inhibitory inputs or whether cortical cells detect coincidences in synaptic input at a millisecond or finer time scale. Unpublished data from B. Ahmed and K. Martin, printed with permission.

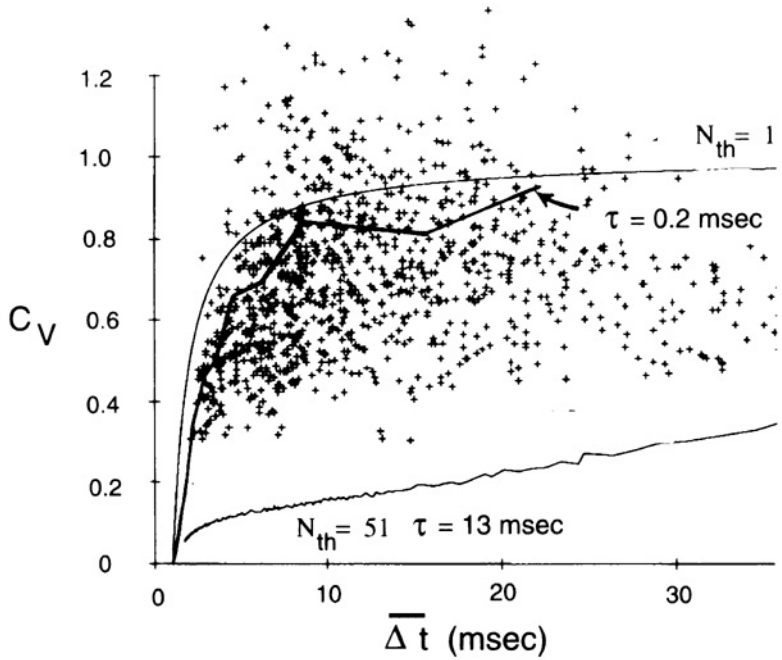


**Fig. 15.9 Firing Variability of Cells in Monkey Cortex** Comparison of the variability of spike timing, quantified using the coefficient of variation $C_V$, as a function of the mean interspike interval for cortical cells and modeled data. The scattered crosses are from V1 and MT cells recorded in the behaving monkey and are normalized for their mean firing rates. Their $C_V$ is high, close to unity. Superimposed are the $C_V$ curves computed for a random walk leaky integrate-and-fire model using conventional assumptions (lower trace; $n_{\text{th}} = 51$, $\tau = 13$ msec, and $t_{\text{ref}} = 1$ msec) and less conventional ones (middle bold trace; $n_{\text{th}} = 51$ and $\tau = 0.2$ msec). The thin, top curve corresponds to the limiting case of a pure Poisson spike train ($n_{\text{th}} = 1$) in combination with $t_{\text{ref}} = 1$ msec. The effect of this absolute refractory period is to render the spike timing very regular at very high firing rates. Reprinted in modified form by permission from Softky and Koch (1993)

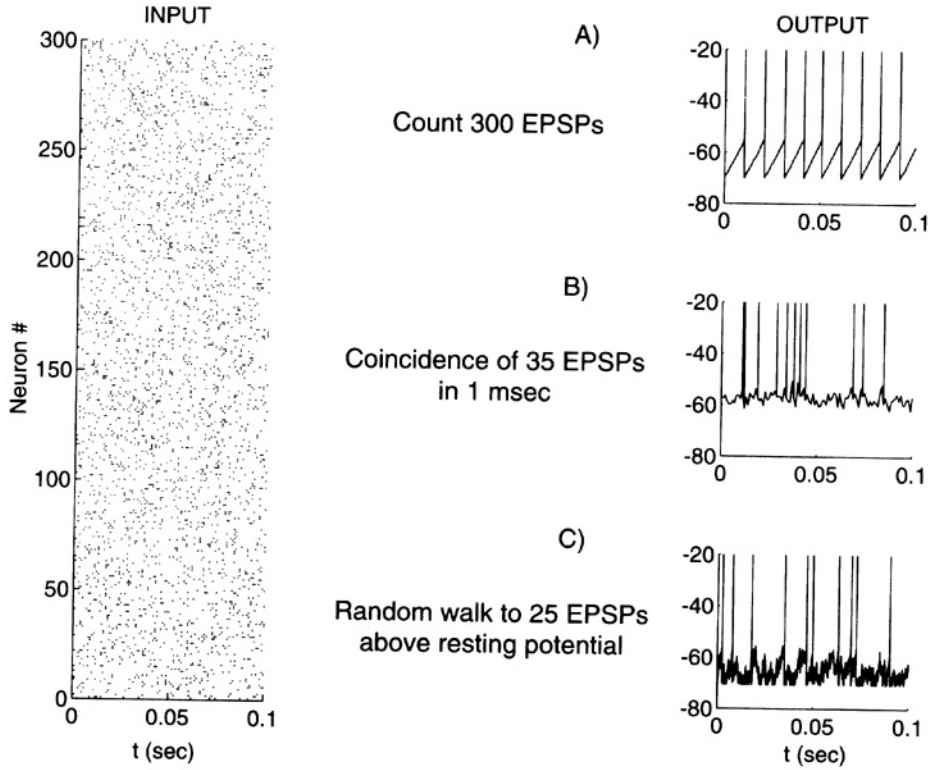


**Fig. 15.10 Three Models of Synaptic Integration** The input to the simulated neuron is shown in the left panel: 300 excitatory Poisson distributed synaptic inputs, firing at a mean rate of $\mu_e = 100$ Hz. The output units on the right also fire at this average rate. **(A)** Ideal integrate-and-fire model. Each synaptic input increases $V$ by 0.05 mV, corresponding to $n_{\text{th}} = 300$. As expected, the output pulses have a clocklike regularity. **(B)** In this cartoon of a coincidence detector model, only inputs within the previous millisecond contribute toward $V$ (corresponding to an effective submillisecond time constant). If $n_{\text{th}} = 35$ EPSPs arrive "simultaneously" (here, within 1 msec), the unit spikes. Notice the elevated mean membrane potential. In this model, the timing of spikes can code information. **(C)** Standard random walk model with a balance of excitation and inhibition. In addition to the 300 excitatory inputs, 150 inhibitory inputs have been added, firing at the same rate; $a_e = 0.6$ mV (corresponding to an effective $n_{\text{th}} = 25$) and $a_i = 1.2$ mV. This model achieves a high variability but at a cost of substantial inhibition. Since no information is encoded in the time of arrival of spikes, it is very robust. Adding a leak term to the first and third models does not affect these conclusions substantially. Reprinted by permission from Shadlen and Newsome (1994)

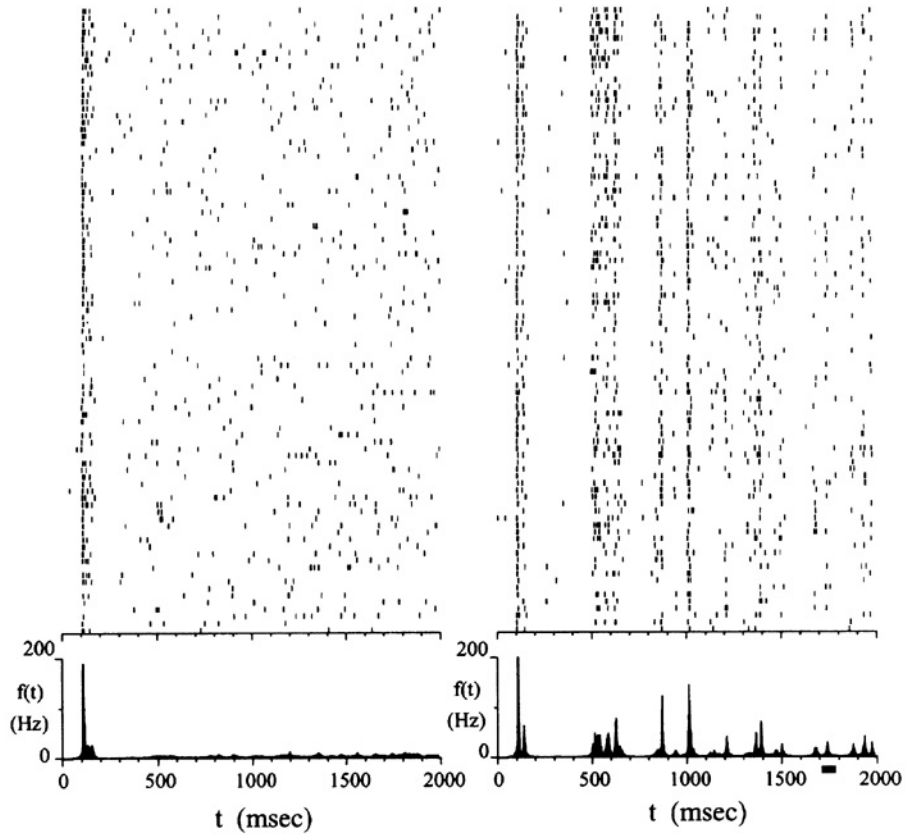


**Fig. 15.11 Cortical Cells Can Fire in a Very Precise Manner** Responses of an MT cell in a behaving monkey to patterns of randomly and independently moving dots. The left column shows the cortical response to different random dot patterns. Averaged over 90 trials, the cell's response is well described by a random point process with $\mu = 3.4$ Hz (excluding the initial "flash" response; see the bottom panel). When only trials over the 2-hour-long experiment that were stimulated by the identical random dot movie are considered (right column), strikingly repeating patterns can be observed. (Viewing this figure obliquely best reveals the precision of spiking.) Notice the sharp peak following the 1-sec mark or that nearly all spikes in the final 400 msec cluster into six vertical streaks. Despite this precision, observed in the majority of MT cells, spike count variability $F(T)$ is still very high. The poststimulus time histogram, using an adaptive square window, is shown at the bottom. Reprinted by permission from Bair and Koch (1996).